Determination of the Orientation Parameters and the Raman Tensor of the 998 cm^{-1} Band of Poly(ethylene terephthalate)

Shuying Yang and Stephen Michielsen*

School of Textile and Fiber Engineering, Georgia Institute of Technology, Atlanta, Georgia 30332-0295

Received April 29, 2002; Revised Manuscript Received October 9, 2002

ABSTRACT: Polarized Raman spectroscopy was used to determine the crystal orientation in uniaxially oriented fibers of poly(ethylene terephthalate) (PET). The Raman tensor ratios and the second- (P_2) and fourth-order (P_4) Legendre polynomials of the orientation distribution function of the 998 cm^{-1} vibrational band are reported. We show that both P_2 and P_4 for this band increase more rapidly than the average chain orientation as determined by birefringence. In addition, they reach plateau values of $P_2 = 0.90 \pm 0.06$ and $P_4 = 0.55 \pm 0.09$ for birefringence values >0.05 in our drawn and annealed samples. Since this band has been assigned to the all-trans conformation of the glycol unit, we suggest that these P_2 and P_4 values correspond to the orientation of the crystalline units. This is the first time that the orientation parameters of the crystals of PET as determined by polarized Raman spectroscopy have been reported.

Introduction

Poly(ethylene terephthalate) (PET) is a semicrystalline polymer with crystallinity ranging from 0 to about 60%. It is widely used to produce fibers, films, and containers. The physical properties of the product depend strongly on the detailed morphology of the material. Here we use "morphology" to refer to the degree of orientation of the polymer molecules and the level of crystallinity. Many techniques such as polarized Raman spectroscopy, polarized fluorescence, NMR, interference microscopy, and X-ray diffraction have been used to measure the orientation of the polymer chains. Among them, polarized Raman microscopy is unique in that it can provide both the second- and fourth-order Legendre polynomials, P_2 and P_4, which describe the orientation, for particular *vibrations* within the samples. Since Bower developed the theory and the procedures for determining the orientation of polymer samples by polarized Raman spectroscopy in 1972,[1] several studies have been performed on PET samples.[2−10] These studies found that the vibrational bands 1616 and 631 cm^{-1} are related to the benzene ring in PET. They can provide overall molecular orientation information about the samples. These earlier studies assumed that the Raman tensor ratios of the particular vibrations are known or can be calculated from an isotropic sample. This assumption implies that the Raman tensor is inherent to the structure and the particular vibrational mode and that it does not change with morphology (crystallinity and/or orientation).

If no assumption is made about the Raman tensor, five spectra are required to determine the five unknowns—the three Raman tensor components, P_2, and P_4. In 2000, Lesko et al.[11] collected all five of the intensities needed for fiber characterization and performed the full analysis of 1616 cm^{-1} band. They found that the Raman tensor ratios of that band varied as a function of the spinning speed at which the samples were produced. This observation called into question the use of isotropic values for the Raman tensor when determining orientation.

In this article, we describe the detailed analysis of the 998 cm^{-1} Raman band for PET. From Boerio and Bahl's[12] normal mode study, this band has been assigned to the symmetric stretching of the $O-CH_2$ bond and the stretching of the C−C bond in ethylene glycol units in an all-trans configuration.[13−15] Bahl, Cornell, and Boerio[16] mentioned that the 998 cm^{-1} band increased in intensity during crystallization. Later, Adar and Noether[17] found that the intensity of this band correlated with the crystallinity. We propose to do the full orientation analysis for this band as we believe that it can provide information about crystal orientation.

Theory

The theory for calculating the orientation parameters and the Raman tensor components has been derived explicitly by Bower[1] and summarized by Citra et al.[18] There are five unknown terms: the three principal components of the Raman tensor, α_1, α_2, and α_3; and the two Legendre polynomials, P_2 and P_4, defined below. If the fiber axis is aligned along the laboratory 3-axis, two of these spectra are readily obtained in backscattering mode or right-angle scattering, I_{33} and $I_{31} = I_{13} = I_{23} = I_{32}$. The subscripts describe the laser polarization and the analyzer polarization, respectively. One spectrum, $I_{11} = I_{22}$, can be obtained from backscattering when the fiber axis is aligned along the 1- or 2-axis, respectively. The fourth spectrum, $I_{12} = I_{21}$, is readily obtained from right angle scattering by aligning the fiber axis along the 3-axis, the laser polarization along the 1-axis, and the analyzer along the 2-axis. The fifth required spectrum is obtained by orienting the fiber at 45° to the 3-axis, the laser polarization direction is aligned along the 3-axis, and the analyzer is aligned along the 1-axis.[18] The relationships between these spectra and the ith, jth component of the second-rank Raman tensor, α_{ij}, are shown in eqs 1 and 2 along with the principal components of the Raman tensor. In addition, P_2 and P_4 are given by Bower[1] and Citra et al.[18] Explicitly

* Corresponding author: e-mail Stephen.michielsen@tfe.gatech.edu.

10.1021/ma0206568 CCC: $22.00
Published on Web 11/23/2002

$$I_{33}^{BS}(0) = I_0\sum\alpha_{33}{}^2 = K(A - 2BP_2 + CP_4)$$

$$I_{11}^{BS}(0) = I_0\sum\alpha_{11}{}^2 = K\left(A + BP_2 + \frac{3}{8}CP_4\right)$$

$$I_{31}^{BS}(0) = I_0\sum\alpha_{31}{}^2 = K\left(D - EP_2 - \frac{1}{2}CP_4\right)$$

$$I_{21}^{RAS}(0) = I_0\sum\alpha_{21}{}^2 = K\left(D + EP_2 + \frac{1}{8}CP_4\right) \quad (1)$$

$$I_{31}^{BS}(\gamma) = I_0\sum\left(\frac{1}{2}\alpha_{11}\sin 2\gamma + [\cos^2\gamma - \sin^2\gamma]\alpha_{31} - \frac{1}{2}\alpha_{33}\sin 2\gamma\right)^2 \quad (2)$$

Using $\gamma = 45°$ and simplifying (see Appendix)

$$I_{31}^{BS}(45) = K\left(D - \frac{1}{2}EP_2 + \frac{19}{32}CP_4\right) \quad (3)$$

where the superscript "BS" refers to the backscattering geometry and "RAS" refers to right angle scattering. The number in parentheses refers to the angle the fiber axis makes with the laboratory 3-axis in the 3,1-plane. The scattered light is collected along the 2-axis. $K = I_0N_0\alpha_3{}^2$, $a_1 = \alpha_1/\alpha_3$, $a_2 = \alpha_2/\alpha_3$, and α_1, α_2, α_3 are the principal components of the Raman tensor. I_0 is the incident intensity, N_0 is the number of scatterers within the scattering volume, and P_2 and P_4 are the average values of the second and fourth Legendre polynomial, respectively. They are given by

$$P_2 = \langle P_2(\cos\theta)\rangle = \frac{\langle 3\cos^2\theta - 1\rangle}{2}$$

$$P_4 = \langle P_4(\cos\theta)\rangle = \frac{\langle 35\cos^4\theta - 30\cos^2\theta + 3\rangle}{8} \quad (4)$$

where the angle brackets indicate the average is taken over all chain segments within the scattering volume. The angle θ is the angle between the Raman tensor principal component α_3 and the fiber axis. Finally, A, B, C, D, and E are given by

$$A = \frac{3a_1{}^2 + 3a_2{}^2 + 3 + 2a_1a_2 + 2a_1 + 2a_2}{15}$$

$$B = \frac{3a_1{}^2 + 3a_2{}^2 - 6 + 2a_1a_2 - a_1 - a_2}{21}$$

$$C = \frac{3a_1{}^2 + 3a_2{}^2 + 8 + 2a_1a_2 - 8a_1 - 8a_2}{35}$$

$$D = \frac{a_1{}^2 + a_2{}^2 + 1 - a_1a_2 - a_1 - a_2}{15}$$

$$E = \frac{a_1{}^2 + a_2{}^2 - 2 - 4a_1a_2 + 2a_1 + 2a_2}{21} \quad (5)$$

By solving eqs 1 and 3 simultaneously, the orientation parameters and the Raman tensor components can be obtained.

Experiment

The PET samples were spun with a range of take-up speeds from 2000 to 4500 m/min, drawn to different draw ratios, and then annealed at 150 °C. Single filaments of each of these samples were glued across the opening of $^1/_4$ in. (~6 mm) steel washers. The Raman spectra were obtained using a 10× objective on a Holoprobe Research 785 nm Raman microscope made by Kaiser Optical Systems, Inc. Approximately 3 mW of laser light was focused onto the filaments. Three specimens were used from each sample.

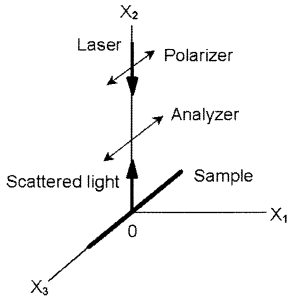

Figure 1. (a) Schematic representation of the Raman backscattering experiment. 0-$X_1X_2X_3$ are the lab coordinates. (The arrangement shown is for the I_{33} spectra.)

Table 1. Experimental Setup for Raman Spectra

	propagation direction		polarization direction		
spectra	incident light[a]	scattered light[a]	incident light[a]	scattered light	fiber axis
I_{11}				X_3	X_1
I_{33}				X_3	X_3
I_{13}	$-X_2$	X_2	X_3	X_1	X_1
I_{31}				X_1	X_3
$I_{31}(45)$				X_1	45° to X_1
I_{23}	X_1	X_2	X_2	X_3	X_3
I_{21}				X_1	X_3

[a] All rows within a single region have the same orientation direction.

Polarized Raman spectra were collected in all five geometries and polarizations. Both backscattering and right-angle scattering modes were used. Figure 1 shows a schematic representation of the Raman polarization experiment showing the arrangement for the I_{33} spectra. Two additional, degenerate spectra were obtained to normalize the I_{21} and the I_{11} spectra to the I_{33} spectra. The symmetry relationship $I_{31} = I_{13}$ was used to correct the I_{11} spectra, and $I_{31} = I_{23}$ was used to correct the I_{21} spectra. The experimental geometries are summarized in Table 1. I_{23} and I_{21} were obtained from right-angle scattering while the other five intensities were collected from backscattering. The five corrected spectra are shown in Figure 2 for sample GT_E specimen 2.

All data acquisition was performed using the Kaiser Optical Systems' "HoloGRAMS" software. HoloGRAMS was responsible for setup, calibration, and operation of the HoloProbe unit. Spectra acquired by HoloGRAMS were then transferred to the GRAMS32 software package (Galactic Industries Inc.) for analysis. The imbedded curve-fit routine was used to fit the peaks and gave the center, height, full width at half-maximum (fwhm), and the Gaussian and Lorentzian content for each peak. The area under the peak was taken as the intensity of the peak. The raw peak intensities were corrected for differences in focus, laser power variation, CCD response, the fiber-optic efficiency, and the instrumental factor, which is due to a difference in the sensitivity of the instrument for different polarizations.

The birefringence, Δn, and the Lorentz densities, ρ, were determined by applying the functions developed previously by Natarajan and Michielsen:[19,20]

$$\Delta n = 0.001 + 0.0267(I_{33,998}/I_{33,702}) + 0.00047(I_{33,1616}/I_{33,702})^2 \quad (6)$$

$$\rho = 1.402 + 0.00177(I_{33,998}/I_{33,702}) - 0.024(\mathrm{fwhm}_{33,1725}) + 0.00083(I_{33,998}/I_{33,702})^2 \quad (7)$$

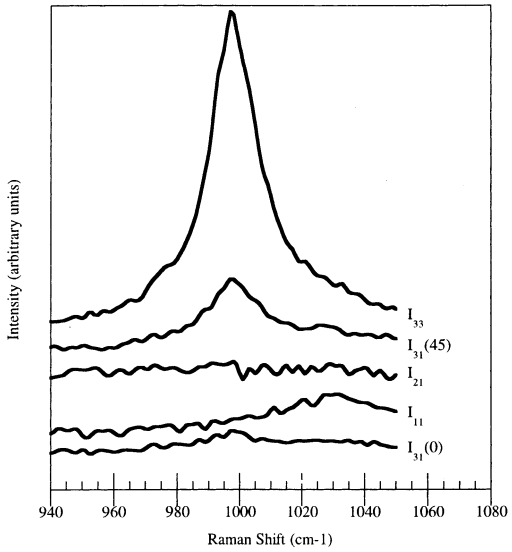

Figure 2. Five corrected Raman spectra of the 998 cm^{-1} band are shown for sample GT_E specimen 2.

where $I_{33,xxx}$ is the intensity of the *xxx* cm^{-1} Raman band in the 33 geometry and $fwhm_{33,1725}$ is the full width at half-maximum of the 1725 cm^{-1} Raman band in the 33 geometry.

Once the birefringence of the samples has been determined, Kashiwagi et al.'s analysis[2,21,22] can be used to obtain the second-order orientation parameter P_2 for the chains:

$$P_{2,\Delta n} = \Delta n/\Delta_{max} \tag{8}$$

where the subscript "*nv*" refers to P_2 obtained from birefringence and Δ_{max} is the maximum birefringence for the fully oriented chains. For PET, $\Delta_{max} = 0.245$.[2]

All seven spectra from the different geometries and polarizations were collected and analyzed. The spectra were corrected for the difference in sensitivity of the instrument to the different polarizations. In addition, the raw intensities were normalized to the I_{31} intensity according to eq 9 using the identity $I_{31} = I_{13} = I_{32} = I_{23}$ for cylindrical symmetry. Thus

$$I_{11}^{corr} = \frac{I_{31}}{I_{13}} I_{11}$$

$$I_{21}^{corr} = \frac{I_{31}}{I_{32}} I_{21} \tag{9}$$

The $I_{31}^{BS}(45)$ spectra were corrected for the instrumental factor but not for the change in orientation as there is no simple equation equivalent to eq 10 for this geometry. Both the $I_{11}(0)$ and the $I_{31}(45)$ are obtained by rotating the fiber about the laser axis by 90° and 45°, respectively. When the I_{33}, I_{31}, I_{13}, and I_{11} spectra have been collected in sequence, the coefficient of variation of the ratio I_{31}/I_{13} is less than 10%. Since $I_{31}^{BS}(45)$ was always collected in sequence with I_{33} and I_{31}, the error in its intensity should also be ≤10%. Citra et al.[18] obtained $I_0\Sigma\alpha_{11}\alpha_{33}$ from a combination of three different spectra, and thus the error in their value of $I_0\Sigma\alpha_{11}\alpha_{33}$ is subject to the error in all three spectra. We obtain the same term directly from $I_{31}^{BS}(45)$ and thus should be less susceptible to these additional errors.

Results and Discussion

During the curve-fitting process, we found that the 998 cm^{-1} band is a pure Lorentzian band, suggesting that this vibration originates from a single environment, in other words, from the crystalline region. We also found that this band is highly polarized, and its intensity seems to depend on the crystallinity and thus on the density as observed by Bahl, Cornell, and Boerio[16] and by Adar and Noether.[17] Figure 3 shows the approximately linear relationship between the I_{33} intensity of the 998 cm^{-1} band and the crystallinity of the samples calculated from the Lorentz density:

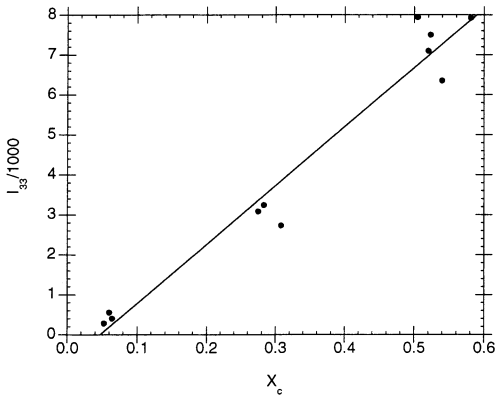

Figure 3. I_{33} intensity of the 998 cm^{-1} vibrational band is seen to increase linearly with the crystallinity.

$$X_c = \frac{\rho - \rho_a}{\rho_c - \rho_a} \tag{10}$$

where X_c is the fractional crystallinity, $\rho_a = 1.335$ g/cm^3 is the density of the amorphous nonoriented phase, and $\rho_c = 1.455$ g/cm^3 is the density of the crystalline phase.[23] According to eq 1, if P_2, P_4, α_1, α_2, and α_3 are constants, then $I_{33} = \kappa I_0 N_0$, where κ is a constant. Since the vast majority of chain segments in the all-trans configuration of the ethylene glycol unit are expected to lie within the crystals, and since N_0 is just the number of chain segments in the all-trans configuration of the ethylene glycol unit within the scattering volume, N_0 should be directly proportional to the crystallinity. From the observed linear relationship between I_{33} and X_c, and hence with N_0, we believe this band has the potential to provide information about crystal orientation as shown below. The full analysis will be discussed further below, and it will be seen that the conditions P_2, P_4, α_1, and α_3 = constants are satisfied in most samples, while $\alpha_2 \neq$ constant.

By solving eqs 1 and 3 simultaneously, the orientation parameters P_2 and P_4 of the 998 cm^{-1} band were obtained, along with a_1, a_2, and K. In Figure 4, both P_2 and P_4 of the 998 cm^{-1} band are plotted against birefringence. The values of $P_{2,998}$ range from 0.26 to 0.99 while P_4 from −0.24 to 0.69. For samples with low birefringence, both P_2 and P_4 increase with the overall orientation of the samples. However, in our samples when the birefringence is greater than 0.05, P_2 and P_4 are nearly constant, $P_2 = 0.90 \pm 0.06$ and $P_4 = 0.56 \pm 0.09$. For all samples, P_2 is greater than P_4. This is the first time that orientation parameters of the all-trans conformation of the ethylene glycol unit of PET have been reported from polarized Raman microscopy.

In Figure 5, $P_{2,998}$ and the overall chain orientation parameter $P_{2,\Delta n}$ are compared by plotting them as functions of birefringence of the samples. In all cases, $P_{2,998}$ is higher than $P_{2,\Delta n}$. This means that the ethylene glycol units in the all-trans conformation make a smaller angle to the fiber axis than the average angle of all chain segments. Since PET crystallizes slowly *except* when oriented, these results can be understood as follows. When the chain segments are oriented by

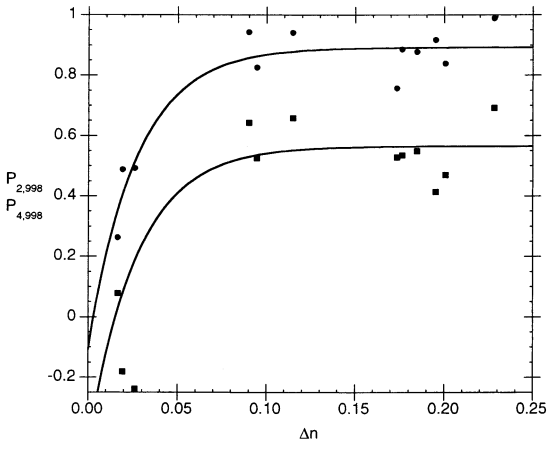

Figure 4. Legendre polynomial values, (●) P_2 and (■) P_4, of the 998 cm^{-1} vibrational band are shown compared to the birefringence.

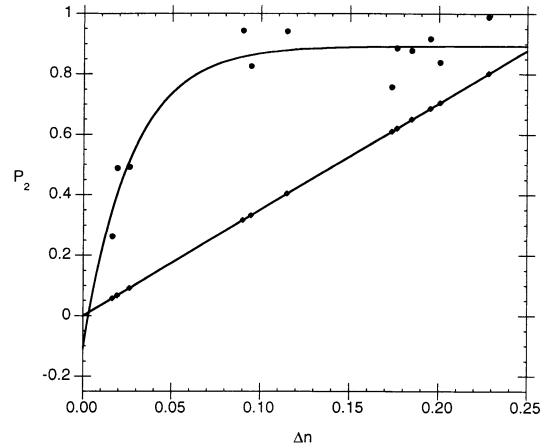

Figure 5. Comparison of (●) $P_{2,998}$ and (◆) $P_{2,\Delta n}$ for the PET. $P_{2,\Delta n}$ is P_2 determined from the birefringence.

the elongation of the polymer melt, they crystallize many orders of magnitude faster than the unoriented chain segments.[24] Thus, the crystals are expected to be highly oriented. In addition, the chains in the crystalline region will be in the all-trans conformation of the ethylene glycol unit. Since most of the chains in the all-trans conformation will be oriented and since they crystallize rapidly when oriented, $P_{2,998}$ and $P_{4,998}$ should provide good measures of the crystalline orientation.

The samples shown in Figure 5 with large P_2 and P_4 were made by drawing and annealing the fibers under tension. These fibers were also spun at higher speeds than the sample with $P_2 < 0.6$, which was spun at 1000 m/min and was not annealed. Drawing the samples results in higher orientations of the chains. This increased orientation of the chains nucleates crystallization within the samples while annealing them allows the crystals to grow. Growth rates of crystals from oriented chain segments in PET is estimated from experitments to be more than 5 orders of magnitude faster than unoriented PET, while theory suggests rates more than 10 orders of magnitude faster. Thus, the crystals are more highly oriented than the noncrystalline regions.[25] The X-ray work of Desai[25] shows that the stress-oriented crystallization of PET for a spinning series results in P_2 of 0.89−0.93. In addition, the crystal orientation for spin orientation-induced crystallization has been determined by measuring the polarized "natural" fluorescence of PET. The crystal orientation was

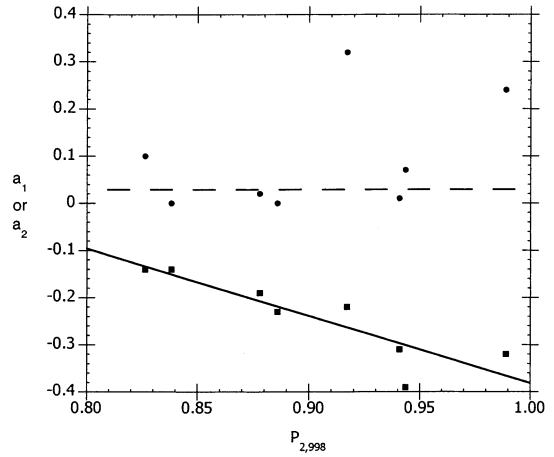

Figure 6. Raman tensor ratios (●) $a_1 = \alpha_1/\alpha_3$ and (■) $a_2 = \alpha_2/\alpha_3$ of the 998 cm^{-1} vibrational band are shown as functions of $P_{2,998}$. The solid line is a straight line fit for a_2 while the dashed line is a horizontal line through the a_1 points, excluding the two high values of a_1.

found to be nearly constant with P_2 reported to lie just above 0.9.[24] (P_2 is equal to Herman's orientation function, f.) Thus, our Raman observations confirm the earlier X-ray and polarized fluorescence results. Namely, after the onset of stress-oriented crystallization, the increase of the crystal *orientation* is small. However, the amount of the crystalline phase continues to increase with spinning speed as indicated by the linear relationship between I_{33} and the crystallinity as shown in Figure 2. This indicates that the high overall orientation $P_{2,\Delta n}$ of the highly oriented samples must arise from the increase in crystallinity (where all the crystals are highly oriented) and/or from higher orientation in the noncrystalline region. The orientation parameter of the noncrystalline region can be derived from $P_{2,\Delta n}$ and $P_{2,998}$, once the crystallinity of the samples is known.

Besides the orientation information described above, we have also measured the principal components of the 998 cm^{-1} band Raman tensor. Figure 6 shows the ratios of the principal components, $a_1 = \alpha_1/\alpha_3$ and $a_2 = \alpha_2/\alpha_3$, of the Raman tensor of the 998 cm^{-1} vibration. Unfortunately, because of large errors in the curve fitting of this peak, which is very weak for samples with low orientation and low crystallinity, it is impossible to obtain the a_1 and a_2 parameters for samples with very low orientation. For the remainder of the samples, it appears that a_1 and a_2 are of opposite signs. Although there is considerable scatter, it appears that one of the Raman tensor ratios, a_1, is close to zero and nearly constant while the other one, a_2, is negative and decreases as the crystal orientation P_2 increases. From this series of fibers, it is difficult to draw any conclusions about the trends of a_1 and a_2 with overall orientation or crystallization since this set of samples was spun, postdrawn, and annealed at different speeds, draw ratios, and temperatures. The resulting morphology, orientation, and crystallization of the samples are a complex function of the spin speed and draw ratio. By examining a pure spin speed series (in progress), we anticipate more general conclusions can be made for the 998 cm^{-1} absorption.

The third principal component, α_3, is contained in $K = N_0 I_0 \alpha_3^2$, where I_0 is the incident intensity and N_0 is the number of scatterers in the scattering volume, which is proportional to the crystallinity of the samples. To remove the contribution from N_0, we divide K by the

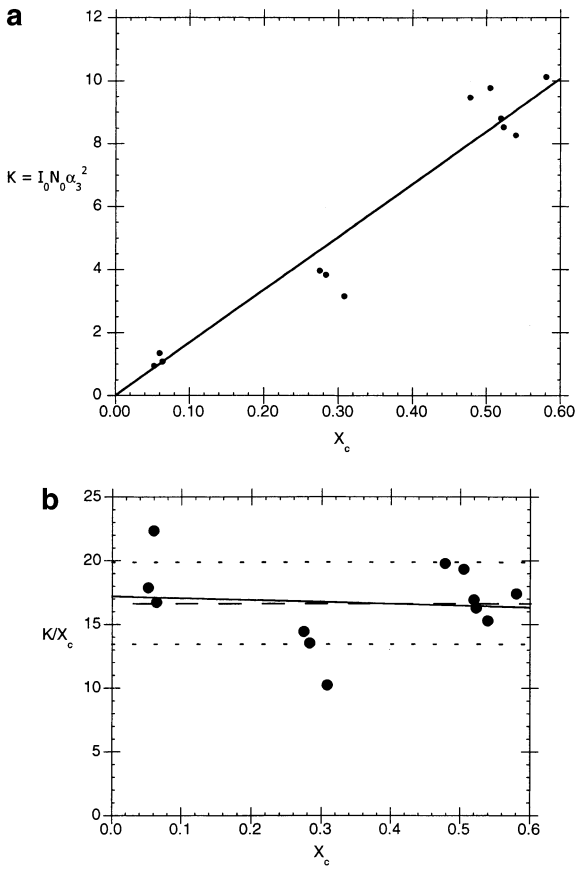

Figure 7. (a) $K = N_0 I_0 \alpha_3^2$ and (b) $K/X_c = I_0 \alpha_3^2$ for the 998 cm^{-1} band are plotted against X_c. The solid line is a linear regression through all of the data, the dashed line is the average value of the data, and the dotted lines indicate ±1 standard deviation from the average.

crystallinty, X_c. Since the incident intensity does not depend on the crystallinity of the samples and its variation is small, the quantity K/X_c should be proportional to a_3^2. In Figure 7a, K for the 998 cm^{-1} band is plotted against X_c of the samples. There is a strong linear relationship between $K = N_0 I_0 \alpha_3^2$ and X_c. On the other hand, Figure 7b shows that there is little or no correlation between $K/X_c = I_0 \alpha_3^2$. In other words, a_3^2 is not sensitive to the extent of crystallinity for the samples studied. Thus, the dependence of K on X_c is entirely through N_0, which confirms our supposition that the 998 cm^{-1} Raman band can be used to measure the crystallinity.

We are performing a similar analysis on PET fibers in which only the spinning speed has been varied. We hope to gain a better understanding of the dependence of the crystal orientation on the processing conditions. This should provide insight into the dependence of the orientation of the noncrystalline regions on the processing conditions. The knowledge of the orientation distribution function of polymer chains in the noncrystalline fraction of the fibers should allow us to ascertain the dependence of the modulus of the noncrystalline region on the orientation distribution of the polymer chains and on processing conditions.

Conclusions

Polarized Raman spectroscopy was used to analyze the 998 cm^{-1} band, which is associated with the all-trans conformation of the glycol unit in PET. We observed that the I_{33} spectral intensity of this band has a linear relationship with crystallinity of the samples. We found that the crystal orientation, $P_{2,998}$, increases much faster with the overall orientation of the samples than does the average chain orientation. We also found that after the onset of stress-oriented crystallization the increase of the orientation of the crystals is small with $P_{2,998} = 0.90 \pm 0.06$ and $P_{4,998} = 0.55 \pm 0.09$. Additionally, we observed that the two Raman tensor ratios of this band appear to be of opposite signs. $a_1 = \alpha_1/\alpha_3$ is constant while $a_2 = \alpha_2/\alpha_3$ decreases with increasing crystal orientation. The square of the third principal component of the Raman tensor, α_3^2, is independent of crystallinity for this sample series. Finally, $K = N_0 I_0 \alpha_3^2$ depends linearly on X_c, indicating that N_0, or the number of all-trans conformations of the ethylene glycol units, is directly proportional to the crystallinity. Thus, the crystallinity and the crystal orientation can be determined from a full analysis of the 998 cm^{-1} vibrational band using Raman spectroscopy.

Acknowledgment. The authors thank the National Textile Center (Department of Commerce) for funding this research and Dr. Prashant Desai for providing the polyester samples.

Appendix

The transformation from eq 2 to eq 3, although not obvious, is straightforward. We start with start with eq 2, which is repeated below:

$$I_{31}^{BS}(\gamma) = I_0 \sum \left(\frac{1}{2}\alpha_{11} \sin 2\gamma + [\cos^2\gamma - \sin^2\gamma]\alpha_{31} - \frac{1}{2}\alpha_{33} \sin 2\gamma \right)^2 \quad \text{(A-1)}$$

For $\gamma = 45°$, $\cos^2\gamma - \sin^2\gamma = 0$. Then

$$I_{31}^{BS}(45) = \frac{1}{4} I_0 \sum \alpha_{11}^2 - \frac{1}{2} I_0 \sum \alpha_{11}\alpha_{33} + \frac{1}{4} I_0 \sum \alpha_{33}^2 \quad \text{(A-2)}$$

The first and the last terms on the right-hand side (rhs) of eq A-2 can be obtained from eq 1 in the text:

$$I_{31}^{BS}(45) = \frac{1}{4}\left[K\left(A + BP_2 + \frac{3}{8}CP_4\right)\right] - \frac{1}{2} I_0 \sum \alpha_{11}\alpha_{33} + \frac{1}{4}[K(A - 2BP_2 + CP_4)] \quad \text{(A-3)}$$

Combining the first and third rhs terms

$$I_{31}^{BS}(45) = \frac{1}{2}K\left(A - \frac{1}{2}BP_2 + \frac{11}{16}CP_4\right) - \frac{1}{2} I_0 \sum \alpha_{11}\alpha_{33} \quad \text{(A-4)}$$

The second term on the rhs can be obtained from eq 9 of Citra et al.[18] In our notation it becomes

$$I_0 \sum \alpha_{11}\alpha_{33} = K\left\{ \frac{1}{15}(a_1^2 + a_2^2 + 1 + 4a_1a_2 + 4a_1 + 4a_2) - \frac{P_2}{42}(a_1^2 + a_2^2 - 2 + 10a_1a_2 - 5a_1 - 5a_2) - \frac{P_4}{70}(3a_1^2 + 3a_2^2 + 8 + 2a_1a_2 - 8a_1 - 8a_2) \right\} \quad \text{(A-5)}$$

The third term on the rhs is simply $-KCP_4/2$, the second term is $-K(B - 2E)P_2/2$, and the first term is

$K(A - 2D)$. Substituting these into (A-4) gives

$$I_0 \sum \alpha_{11}\alpha_{33} = K\left\{(A - 2D) - \frac{P_2}{2}(B - 2E) - \frac{P_4}{2}C\right\} \quad \text{(A-6)}$$

Finally, substituting (A-6) into (A-4) gives

$$I_{31}^{BS}(45) = \frac{1}{2}K\left(A - \frac{1}{2}BP_2 + \frac{11}{16}CP_4\right) - \frac{1}{2}K\left\{(A - 2D) - \frac{P_2}{2}(B - 2E) - \frac{P_4}{2}C\right\} \quad \text{(A-7)}$$

Combining terms gives eq A-8, which is identical to eq 3:

$$I_{31}^{BS}(45) = K\left(D - \frac{1}{2}EP_2 + \frac{19}{32}CP_4\right) \quad \text{(A-8)}$$

References and Notes

(1) Bower, D. I. *J. Polym. Sci., Polym. Phys. Ed.* **1972**, *10*, 2135−2153.
(2) Purvis, J.; Bower, D. I.; Ward, I. M. *Polymer* **1973**, *14*, 398−400.
(3) Purvis, J.; Bower, D. I. *J. Polym. Sci., Polym. Phys. Ed.* **1976**, *14*, 1461−1484.
(4) Nobbs, J. H.; Bower, D. I.; Ward, I. M. *J. Polym. Sci., Polym. Phys. Ed.* **1979**, *17*, 259−272.
(5) Jarvis, D. A.; Hutchinson, I. J.; Bower, D. I.; Ward, I. M. *Polymer* **1980**, *21*, 41−54.
(6) Bower, D. I.; Jarvis, D. A.; Ward, I. M. *J. Polym. Sci., Polym. Phys. Ed.* **1986**, *24*, 1459−1479.
(7) Bower, D. I.; Jarvis, D. A.; Lewis, E. L. V.; Ward, I. M. *J. Polym. Sci., Polym. Phys. Ed.* **1986**, *24*, 1481−1492.
(8) Bower, D. I.; Ward, I. M. *Polymer* **1982**, *24*, 645−649.
(9) Lapersonne, P.; Bower, D. I.; Ward, I. M. *Polymer* **1992**, *33*, 1266−1276.
(10) Everall, N. J. *Appl. Spectrosc.* **1998**, *52*, 1498−1504.
(11) Lesko, C. C. C.; Rabolt, J. F.; Ikeda, R. M.; Chase, B.; Kennedy, A. *J. Mol. Struct.* **2000**, *521*, 127−136.
(12) Boerio, F. J.; Bahl, S. K. *J. Polym. Sci., Polym. Phys. Ed.* **1976**, *14*, 1029−1046.
(13) Stokr, J.; Schneider, B.; Doskocilova, D.; Lovy, J. *Polymer* **1982**, *24*, 714−721.
(14) Everall, N.; Tayler, P.; Chalmers, J. M.; MacKerron, D. *Polymer* **1994**, *35*, 3184−3192.
(15) Quintanilla, L.; Rodriguez-Cabello, J. C.; Pastor, J. M. *J. Raman Spectrosc.* **1994**, *25*, 335−344.
(16) Bahl, S. K.; Cornell, D. D.; Boerio, F. J. *J. Polym. Sci., Polym. Lett. Ed.* **1974**, *12*, 13−19.
(17) Adar, F.; Noether, H. *Polymer* **1985**, *26*, 1935−1943.
(18) Citra, M. J.; Chase, D. B.; Ikeda, R. M.; Gardner, K. H. *Macromolecules* **1996**, *28*, 4007−4012.
(19) Natarajan, S.; Michielsen, S. *J. Appl. Polym. Sci.* **1999**, *73*, 943−952.
(20) Natarajan, S. Characterization of Poly(ethylene terephthalate) Fibers Using Raman Microscopy. Master Thesis, Georgia Institute of Technology, 1998.
(21) Kashiwagi, M.; Cunningham, A.; Manuel, A.; Ward, I. M. *Polymer* **1973**, *14*, 111−124.
(22) Foot, J. S.; Ward, I. M. *J. Mater. Sci.* **1975**, *10*, 955−960.
(23) Rule, M. In *Polymer Handbook*; Brandrup, J., Immergut, E. H., Grulke, E. A., Eds.; John Wiley and Sons: New York, 1999; p V113.
(24) Spruiell, J. E. In *Structure Formation in Polymeric Fibers*; Salem, D. R., Ed.; Hanser Gardner Publications: Cincinnati, OH, 2001; pp 53−55.
(25) Desai, P. Fundamental Aspects of Crystallization and Thermorheological Behavior of Uniaxially Oriented Polymers. Ph.D. Thesis, Georgia Institute of Technology, 1988.

MA0206568